

Application of simulated tempering and magnetizing to a two-dimensional Potts model

This article has been downloaded from IOPscience. Please scroll down to see the full text article.

J. Stat. Mech. (2013) P02039

(<http://iopscience.iop.org/1742-5468/2013/02/P02039>)

View [the table of contents for this issue](#), or go to the [journal homepage](#) for more

Download details:

IP Address: 133.6.213.40

The article was downloaded on 28/02/2013 at 00:46

Please note that [terms and conditions apply](#).

Application of simulated tempering and magnetizing to a two-dimensional Potts model

Tetsuro Nagai¹, Yuko Okamoto^{1,2,3,4} and Wolfhard Janke⁵

¹ Department of Physics, Graduate School of Science, Nagoya University, Nagoya, Aichi 464-8602, Japan

² Structural Biology Research Center, Graduate School of Science, Nagoya University, Nagoya, Aichi 464-8602, Japan

³ Center for Computational Science, Graduate School of Engineering, Nagoya University, Nagoya, Aichi 464-8603, Japan

⁴ Information Technology Center, Nagoya University, Nagoya, Aichi 464-8601, Japan

⁵ Institut für Theoretische Physik and Centre for Theoretical Sciences (NTZ), Universität Leipzig, Postfach 100 920, D-04009 Leipzig, Germany

E-mail: tnagai@nagoya-u.jp, okamoto@phys.nagoya-u.ac.jp and Wolfhard.Janke@itp.uni-leipzig.de

Received 14 December 2012

Accepted 6 January 2013

Published 27 February 2013

Online at stacks.iop.org/JSTAT/2013/P02039

[doi:10.1088/1742-5468/2013/02/P02039](https://doi.org/10.1088/1742-5468/2013/02/P02039)

Abstract. We apply the simulated tempering and magnetizing (STM) method to the two-dimensional three-state Potts model in an external magnetic field in order to investigate STM's applicability further. The temperature and the external field are treated as dynamical variables updated during the STM simulations. On the basis of adequate information obtained by STM for several lattice sizes $L \times L$ (up to 160×160), we also perform a number of conventional canonical simulations of larger lattices in order to illustrate the crossover behavior of the Potts model in an external field with increasing L . The temperature and external field for the larger lattice size simulations are chosen by extrapolation of the detailed information obtained by STM. We present a careful analysis of the crossover-scaling behavior at the phase transitions with respect to the lattice size as well as the temperature and external field. The crossover behavior is clearly observed in the simulations in agreement with theoretical predictions.

Keywords: classical Monte Carlo simulations, classical phase transitions (theory), finite-size scaling, sampling algorithms and rapid mixing

ArXiv ePrint: [1212.3084](https://arxiv.org/abs/1212.3084)

Contents

1. Introduction	2
2. The model and methods	3
2.1. The model	3
2.2. The simulation methods	5
2.3. Free energy calculations	8
3. Results and discussion	10
4. Conclusions	18
Acknowledgments	20
References	20

1. Introduction

Monte Carlo (MC) and molecular dynamics (MD) computer simulation methods have been demonstrated in many applications to be indispensable tools for studying the statistical properties of various physical systems in equilibrium. The quasi-ergodicity problem, however, where the system gets trapped in states of local energy minima, has often posed great difficulties. In order to overcome this difficulty, generalized-ensemble algorithms have been developed and applied to many problems in spin models and biomolecular systems (for reviews, see, e.g., [1]–[4]).

Well-known examples of generalized-ensemble algorithms are the multicanonical algorithm (MUCA) [5, 6], simulated tempering (ST) [7, 8], and the replica-exchange method (REM) [9, 10] (also referred to as parallel tempering). Closely related to MUCA are the Wang–Landau method [11, 12] and so-called metadynamics [13]. REM is implicitly a special case of the more general method described in the earlier work of [14], as shown later in [15].

On the basis of the recent multi-dimensional generalization of generalized-ensemble algorithms [16]–[18], the ‘simulated tempering and magnetizing’ (STM) method has been proposed and developed [19, 20]. In [19, 20] two of us studied the classical Ising model, introducing the external (magnetic) field as a second dynamical variable, besides the temperature, and showed improvements over the conventional ‘one-dimensional’ ST schemes, such as better sampling efficiency and potential applicability to a first-order phase transition, which cannot be dealt with by one-dimensional ST.

In the present work, we further investigate the STM method by applying it to the two-dimensional three-state Potts model in an external magnetic field [21, 22]. This model has

several interesting applications in condensed matter physics [22], and its three-dimensional counterpart serves as an effective model for quantum chromodynamics [23]–[26]. We show that the STM scheme works in this more complicated system as well. We also look into the crossover-scaling behavior as regards the dependence on the lattice size L as well as temperature T and external field h . We observe that the STM method enables us to investigate a wide area of sampling space.

The rest of this article is organized as follows. In section 2 we review the STM method and give the details of our simulations. In section 3 we present the results. After checking the two-dimensional random walks, we compare ST and STM, and calculate various thermodynamic quantities for many sets of parameter values, in combination with reweighting techniques. We then use this extensive data set to study the crossover-scaling behavior at the phase transitions with respect to the lattice size as well as the temperature and external field. In section 4 we conclude this paper with a summary and an outlook to future work.

2. The model and methods

2.1. The model

We study the two-dimensional three-state Potts model in an external field with energy:

$$H = E - hM, \tag{1}$$

$$E = - \sum_{\langle i,j \rangle} \delta_{\sigma_i, \sigma_j}, \tag{2}$$

$$M = \sum_{i=1}^N \delta_{0, \sigma_i}, \tag{3}$$

where $N = L^2$ denotes the total number of spins, δ is the Kronecker delta function, σ_i a spin at the i th site, and h the external field. The spin σ_i takes on one of the three values 0, 1, or 2. The sum in (2) runs over all nearest-neighbor pairs, with the spins σ_i arranged on the sites of a square $L \times L$ lattice with periodic boundary conditions. Data were obtained by means of STM for lattice sizes ranging from 2×2 to 160×160 and additionally with conventional canonical simulations on 320×320 and 640×640 lattices.

We recall that the three-state (standard) Potts model is equivalent to the three-state planar Potts or Z_3 model. We first introduce a spin

$$\vec{s}_i = \begin{pmatrix} \cos \frac{2\pi}{3} \sigma_i \\ \sin \frac{2\pi}{3} \sigma_i \end{pmatrix}. \tag{4}$$

The zero-field energy term is then given by

$$E_{\text{planar}} = - \sum_{\langle i,j \rangle} \vec{s}_i \cdot \vec{s}_j, \tag{5}$$

and the magnetization reads

$$\vec{M} = \sum_{i=1}^N \vec{s}_i. \quad (6)$$

In an external field chosen along the x -direction,

$$\vec{h} \equiv h\vec{e}_x, \quad (7)$$

the inner product of the external field and magnetization becomes

$$\vec{h} \cdot \vec{M} = hM^{(x)}, \quad (8)$$

where $M^{(x)}$ stands for the x -component of \vec{M} , which is given by $\sum_i \cos(2\pi/3)\sigma_i$. Because the argument of the cosine and sine in (4) can only take the values of 0, $2\pi/3$, and $4\pi/3$, we have

$$E = (E_{\text{planar}} - N) \times \frac{2}{3}, \quad (9)$$

$$M = \left(M^{(x)} + \frac{N}{2} \right) \times \frac{2}{3}. \quad (10)$$

Thus, we arrive at

$$E - hM = \frac{2}{3}E_{\text{planar}} - \frac{2}{3}hM^{(x)} - \frac{N}{3}(2 - h). \quad (11)$$

Since the last term is an unimportant constant, the standard Potts model is equivalent to the planar Potts model with a $\frac{2}{3}$ -smaller coupling constant and magnetization normalized by $\frac{2}{3}$:

$$H = E - hM, \quad (12)$$

$$E = -\frac{2}{3} \sum_{\langle i,j \rangle} \cos \theta_{ij}, \quad (13)$$

$$M = \frac{2}{3} \sum_{i=1}^N \cos \theta_i, \quad (14)$$

where $\theta_{ij} = \theta_j - \theta_i$ and $\theta_i = (2\pi/3)\sigma_i$.

Because $M^{(x)}$ is the projection of \vec{M} onto the x -axis, $M^{(x)}$ equals N when the system is ordered in the 0-direction and $-N/2$ when it is ordered in the 1-direction or 2-direction (see figure 1). The disordered phase is signaled by $M^{(x)} = 0$. According to (10) this corresponds to $M = N$ for the ordered state in the 0-direction, $M = 0$ for the ordered states in the 1-direction or 2-direction, and $M = N/3$ for the disordered phase.

As one can see from (1) and (3) (or (12) and (14)), spin direction 0 is favored by a positive external field ($h > 0$). Accordingly, a negative external field ($h < 0$) disfavors spin direction 0 and the system is expected to behave like a two-dimensional Ising model. In fact, in the limit $h \rightarrow -\infty$, the three-state Potts model is equivalent to the Ising model in zero external field, because the unfavored states are completely suppressed. Figure 1 illustrates the schematic picture of this relation.

For reference, we summarize the critical exponents for the two-dimensional Ising and three-state Potts models in table 1.

Simulated tempering and magnetizing of a Potts model

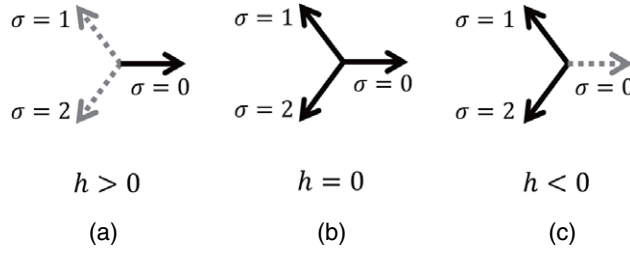


Figure 1. Schematic description of the behavior of the spins according to the external field. (a) Spin 0 is favored for $h > 0$, i.e., spin 1 and spin 2 are disfavored. (b) All three states are equivalent for $h = 0$. (c) Spin 0 is disfavored for $h < 0$.

Table 1. Critical exponents for the two-dimensional Ising and three-state Potts models ($y_t = 1/\nu$, $y_h = (\beta + \gamma)/\nu$) [22].

Model	y_t	y_h	β	γ	δ	ν
Ising	1	15/8	1/8	7/4	15	1
Potts	6/5	28/15	1/9	13/9	14	5/6

2.2. The simulation methods

In this section we briefly review the STM method [19, 20]. While in the conventional ST scheme [7, 8] only the temperature is considered as a dynamical variable, the STM method employs the external field as a second dynamical variable, besides temperature. The STM method is thus based on the multi-dimensional extension of generalized-ensemble algorithms [16]–[18] where one considers

$$e^{-(E-hM)/T+a(T,h)} \tag{15}$$

as a joint probability for $(x, T, h) (\in X \otimes \{T_1, T_2, \dots, T_{N_T}\} \otimes \{h_1, h_2, \dots, h_{N_h}\})$. Here, $a(T, h)$ is a parameter, x denotes a (microscopic) state, and X denotes the sampling space. We have set Boltzmann’s constant to unity. Note that the temperature and external field are discretized into N_T and N_h values, respectively.

A suitable candidate for $a(T_i, h_j)$ may be found by looking into the probability of occupying each set of parameter values. It is given by

$$P(T_i, h_j) = \frac{\sum_{k=1}^{N_T} \sum_{l=1}^{N_h} \int dx \delta_{ik} \delta_{jl} e^{-(E(x)-h_l M(x))/T_k+a(T_k,h_l)}}{\sum_{k=1}^{N_T} \sum_{l=1}^{N_h} \int dx e^{-(E(x)-h_l M(x))/T_k+a(T_k,h_l)}} \tag{16}$$

$$= \frac{e^{-f(T_i,h_j)+a(T_i,h_j)}}{\sum_{k=1}^{N_T} \sum_{l=1}^{N_h} e^{-f(T_k,h_l)+a(T_k,h_l)}} \tag{17}$$

$$\propto e^{-f(T_i,h_j)+a(T_i,h_j)}, \tag{18}$$

where

$$e^{-f(T_i,h_j)} = \int dx e^{-(E-h_j M)/T_i}. \tag{19}$$

This shows that the dimensionless free energy $f(T_i, h_j)$ is the proper choice for $a(T_i, h_j)$, in order to generate a uniform distribution of the number of samples according to T and

h . The free energy values can be estimated by a number of methods. For example, one can obtain such values from preliminary simulations and reweighting techniques.

Any thermal average $\langle A \rangle_{T_i, h_j}$ at given T_i ($\in \{T_1, T_2, \dots, T_{N_T}\}$) and h_j ($\in \{h_1, h_2, \dots, h_{N_h}\}$) can be obtained via the conditional expectation $\langle A \rangle_{T_i, h_j} = \langle A | T_i, h_j \rangle_{\text{STM}}$. Namely, we have

$$\langle A \rangle_{T_i, h_j} = \frac{1}{N_{T_i, h_j}} \sum_{k=1}^{N_{T_i, h_j}} A_{T_i, h_j}^k, \quad (20)$$

where N_{T_i, h_j} is the total number of samples obtained at T_i and h_j , and A_{T_i, h_j}^k represents the k th sample at T_i and h_j .

When considering the temperature T and external field h as dynamical variables, they can be updated similarly to the spin σ_i . The Metropolis criterion for updating T and h is given by

$$w(T_i, h_j \rightarrow T_{i'}, h_{j'}) = \min \left(1, \frac{P(T_{i'}, h_{j'})}{P(T_i, h_j)} \right) \quad (21)$$

$$= \min \left(1, \exp \left(- \left(\frac{1}{T_{i'}} - \frac{1}{T_i} \right) E + \left(\frac{h_{j'}}{T_{i'}} - \frac{h_j}{T_i} \right) M + a(T_{i'}, h_{j'}) - a(T_i, h_j) \right) \right). \quad (22)$$

Once an initial state is prepared, STM simulations can be performed by repeating the following two steps: (1) Perform a conventional canonical simulation at fixed T_i and h_j for a certain number of MC sweeps. (2) Update the temperature and/or external field by using (22) with $a(T, h) = f(T, h)$.

In our implementation, in step (2) above either T or h was updated (the choice between T and h was made at random) by using (22) to a neighboring value (the choice between the two possible neighbors was also made at random). Here, one MC sweep consists of $L \times L$ single-spin updates. In the following we refer to the number of MC sweeps performed between parameter updates as the ‘parameter-updating period’.

We remark that, as spins can be updated via a number of algorithms, other schemes for updating the parameters can be employed [27]. There also exists a temperature-updating scheme for ST, using the Langevin algorithm [28].

Table 2 summarizes the conditions for the present STM simulations. According to the previous studies [20, 29, 30], we updated the parameters frequently. That is, we employed very small parameter-updating periods.

In addition, we also performed conventional canonical simulations. Table 3 lists their details. The temperature was chosen by means of extrapolations of the STM results. We estimated the proper temperature by fitting the STM results to $T_{\max} - T_c \propto L^{-1/\nu}$, where T_{\max} is the temperature at which the observables take their maxima. The Greek letter ν denotes the critical exponent of the correlation length. For vanishing external field we fitted the data to the Potts case ($\nu = 5/6$) and in (negative) external field, to the Ising case ($\nu = 1$).

For the spin variables we employed the single-spin update algorithm, that is, we updated spins one by one with the heat-bath algorithm. As a quasi-random-number generator we used the Mersenne Twister [31].

Table 2. Parameter values for the STM simulations.

Lattice size L	5	10	20	40	80	160
Total number of MC sweeps	220915510	216277330	164000000	164000000	436050000	525000000
Parameter-updating period	1	1	1	1	1	1
T_1, \dots, T_{N_T}	0.1, ..., 3.5	0.1, ..., 3.5	0.3, ..., 3.2	0.3, ..., 3.2	0.5, ..., 2.0	0.5, ..., 2.0
h_1, \dots, h_{N_h}	-1.5, ..., 1.5	-1.5, ..., 1.5	-1.5, ..., 1.5	-1.5, ..., 1.5	-1.5, ..., 1.5	-1.0, ..., 0.025
N_T	20	20	40	40	76	95
N_h	21	21	41	41	51	30
N_{data}^a	10	10	10	10	10	10

^a The data were stored every N_{data} MC sweeps.

Table 3. Parameter values for the regular canonical simulations.

Lattice size L	320	640
Total number of MC sweeps ^a	4000 000	4000 000
(T, h) ^b	(0.995 518, 0), (0.995 995, 0), (0.996 490, 0) (1.075 2077, -0.5), (1.077 044, -0.5), (1.078 302, -0.5) (1.101 447, -1.0), (1.102 321, -1.0), (1.103 380, -1.0)	(0.994 985, 0), (0.995 209, 0), (0.995 512, 0) (1.075 672, -0.5), (1.076 181, -0.5), (1.076 936, -0.5) (1.100 386, -1.0), (1.101 043, -1.0), (1.101 811, -1.0)
N_{data} ^c	10	20

^a The number performed for each set of temperature and external field values.

^b Three temperature values for each external field value were used.

^c The data were stored every N_{data} MC sweeps.

2.3. Free energy calculations

The simulated tempering parameters, or free energies, in (15) and (19) can be simply obtained by reweighting techniques applied to the results of preliminary simulation runs [16]–[18], [32]. We used two reweighting methods for the free energy calculations. One method is the multiple-histogram reweighting method, or weighted histogram analysis method (WHAM) [33]–[35], and the other is the multistate Bennett acceptance ratio estimator (MBAR) method [36], which is based on WHAM.

The equations of the WHAM algorithm applied to the system are as follows. For details, the reader is referred to [17, 34, 35]. The density of states (DOS) $n(E, M)$ and free energy $f(T_i, h_j)$ can be obtained from

$$n(E, M) = \frac{\sum_{i=1}^{N_T} \sum_{j=1}^{N_h} n_{T_i, h_j}(E, M)}{\sum_{i=1}^{N_T} \sum_{j=1}^{N_h} N_{T_i, h_j} \exp(f(T_i, h_j) - (E - h_j M)/T_i)}, \quad (23)$$

$$f(T_i, h_j) = -\ln \sum_{E, M} n(E, M) \exp(-(E - h_j M)/T_i), \quad (24)$$

where $n_{T_i, h_j}(E, M)$ is the histogram of E and M at T_i and h_j , and N_{T_i, h_j} is the total number of samples obtained at T_i and h_j . By solving these two equations self-consistently by iteration, we can obtain $n(E, M)$ and $f(T_i, h_j)$. The $n(E, M)$ obtained allows one to calculate any thermal average at arbitrary temperature and external field values. Note that $f(T_i, h_j)$ is determined up to a constant, which sets the zero point of the free energy. Hence $n(E, M)$ is determined up to a normalization constant.

The MBAR is based on the following equations. Namely, by combining (23) and (24), the free energy can be written as

$$f(T_i, h_j) = -\ln \sum_{n=1}^N \frac{\exp(-(E_n - h_j M_n)/T_i)}{\sum_{k=1}^{N_T} \sum_{l=1}^{N_h} N_{T_k, h_l} \exp(f(T_k, h_l) - (E_n - h_l M_n)/T_k)}, \quad (25)$$

where N is the total number of data, N_{T_k, h_l} is the number of samples associated with T_k and h_l , and E_n and M_n denote the energy and magnetization of the n th measurement.

This equation should be solved self-consistently for $f(T_i, h_j)$. Note that, as in WHAM, $f(T_i, h_j)$ is determined up to a constant.

We repeat the preliminary STM simulations and free energy calculations until we finally obtain sufficiently accurate free energy values which let the system perform a random walk in the temperature and external field space during the STM simulation. Once this has been achieved, the final production run is performed.

Note that these two reweighting methods enable us to obtain not only free energy values but also thermodynamic quantities at any temperature and at any external field. Such averages are given by

$$\langle A \rangle_{T,h} = \sum_{n=1}^N W_{na} A(x_n), \quad (26)$$

$$W_{na} = \frac{1}{\langle c_a \rangle} \frac{\exp(-(E_n - hM_n)/T)}{\sum_{k=1}^{N_T} \sum_{l=1}^{N_h} N_{T_k, h_l} \exp(f(T_k, h_l) - (E_n - h_l M_n)/T_k)}, \quad (27)$$

$$\langle c_a \rangle = \sum_{n=1}^N \frac{\exp(-(E_n - hM_n)/T)}{\sum_{k=1}^{N_T} \sum_{l=1}^{N_h} N_{T_k, h_l} \exp(f(T_k, h_l) - (E_n - h_l M_n)/T_k)}. \quad (28)$$

For further details, the reader is referred to [36, 37].

We also used two other methods for free energy calculations. One is given as follows. By substituting $a(T, h)$ in (18) with the estimates for the free energy $\tilde{f}(T, h)$, we obtain

$$P(T, h) \propto e^{-f(T,h) + \tilde{f}(T,h)}, \quad (29)$$

or

$$f(T, h) = \tilde{f}(T, h) - \ln P(T, h) + \text{const}. \quad (30)$$

Here, $P(T, h)$ can be obtained as a histogram at each set of parameter values in a preliminary STM simulation. Thus, this equation enables one to refine the free energy estimates much more easily than using the reweighting methods, because no iterations are required. This method does not work well, however, when $P(T_i, h_j)$ is too small (or $\tilde{f}(T_i, h_j)$ is too far away from the true value) for obtaining samples at (T_i, h_j) , while the reweighting techniques still work.

The other method for the free energy calculations is a Wang–Landau-like scheme [11, 12], where one subtracts a fixed constant from the free energy value being sampled, during preliminary simulations. To be on the safe side, we did not use such data for reweighting techniques which, strictly speaking, require equilibrium data as input. Note that this method also works with inaccurate free energy estimates. Thus, this method works even when the free energy estimates are far away from sufficiently accurate values.

In the present work, we first used the reweighting methods and Wang–Landau-like scheme to obtain rough estimates of the free energy for the entire parameter space. We then used the combination of the reweighting methods and (30) for further refinements of the free energy.

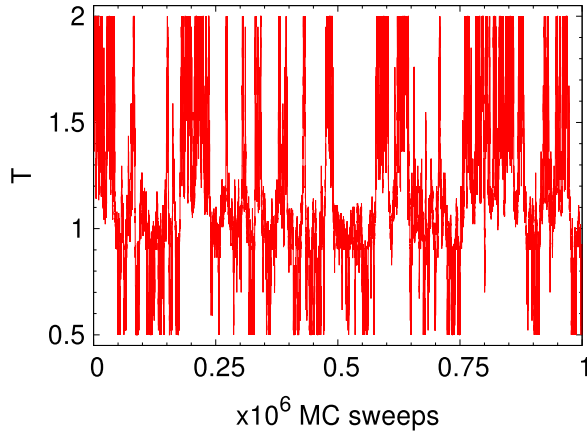


Figure 2. History of temperature T for the linear lattice size $L = 80$.

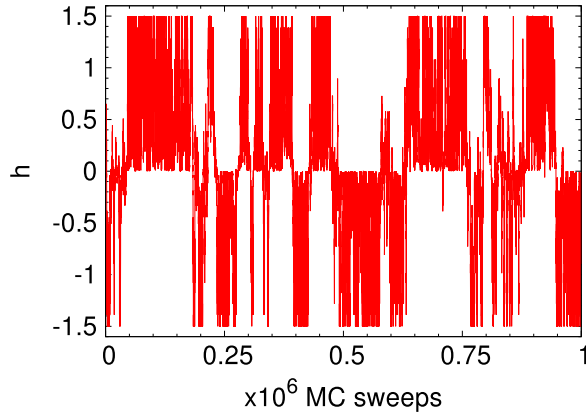


Figure 3. History of external field h for the linear lattice size $L = 80$.

3. Results and discussion

We first examine whether the STM simulations were carried out properly or not. Figures 2 and 3 show the time series for the temperature and external field, respectively, for $L = 80$. In both plots we see block structures reflecting the first-order phase transition line at $h = 0$ in the Potts model (see figure 3) and the second-order phase transition at the effective Ising transition temperature $T_c(h) \approx 1.1346$ for negative external field (see figure 2). Within these blocks, the temperature and external field did indeed realize random walks.

Figures 4 and 5 show the energy and magnetization per spin, respectively, as functions of the number of MC sweeps. Their time evolution also exhibits random-walk-like behavior. Note that there exist expected correlations between the temperature and energy (see figures 2 and 4) and between the external field and magnetization (see figures 3 and 5). The same behavior was observed in simulations with other lattice sizes (data not shown).

Figure 6 shows the history of a differently defined magnetization given by

$$M_{\max} = L^2 m_{\max} \equiv \left\{ \max_{j=0,1,2} \left[\sum_{i=1}^{L^2} \delta_{j,\sigma_i} \right] - \frac{L^2}{3} \right\} \times \frac{3}{2}. \quad (31)$$

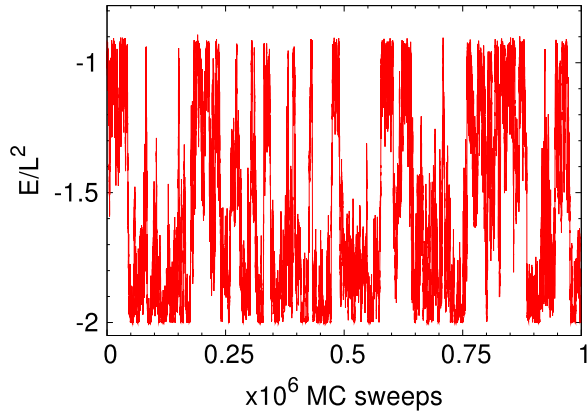


Figure 4. History of the energy per spin, E/L^2 , for the linear lattice size $L = 80$.

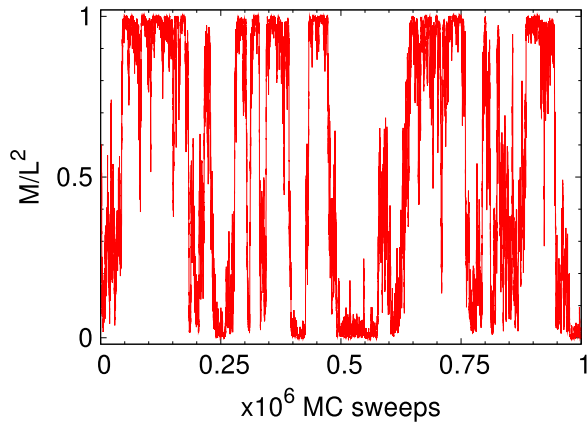


Figure 5. History of the magnetization per spin, M/L^2 , for the linear lattice size $L = 80$. Recall that $M/L^2 = 1$ corresponds to the ordered state in the 0-direction, $M/L^2 = 0$ to the ordered states in the 1-direction or 2-direction, and $M/L^2 = 1/3$ to the disordered state.

This quantity takes the physically more intuitive value of 1 when the system is in one of the three ordered phases and the value 0 for the disordered phase. Here, we see a clear negative correlation between E and M_{\max} (see figures 4 and 6).

In order to compare the results with ordinary ST simulations, we also performed an ST simulation with $L = 40$. The ST simulation was performed with conditions similar to those of STM, namely, the same total number of MC sweeps, same temperature distribution, and so on, except that here we set $h = 0$.

With the data obtained, we performed the WHAM calculations to obtain the DOS. As shown in figure 7, the area sampled by STM is larger than that sampled by ST. Thus, the STM method enables us to perform reweighting techniques over a wider range. We recall that M is zero in the 1-direction or 2-direction ordered phases. The disordered phase corresponds to $M/L^2 = 1/3$.

We further closely looked into the difference in sampled area between the two methods. Figure 8 illustrates how the sampled areas differ. The red region was sampled by the STM method exclusively, the green region by both methods, the blue region by the ST method

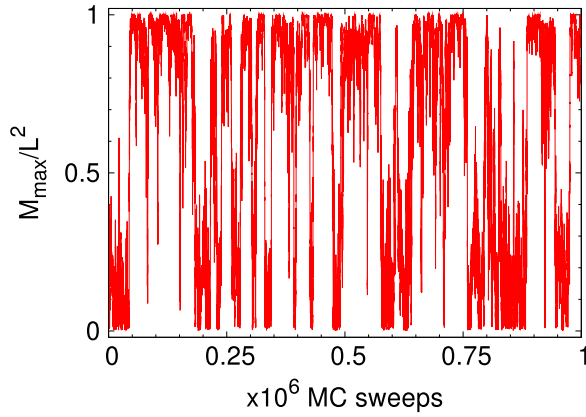


Figure 6. History of M_{\max}/L^2 ($\equiv m_{\max}$), for the linear lattice size $L = 80$.

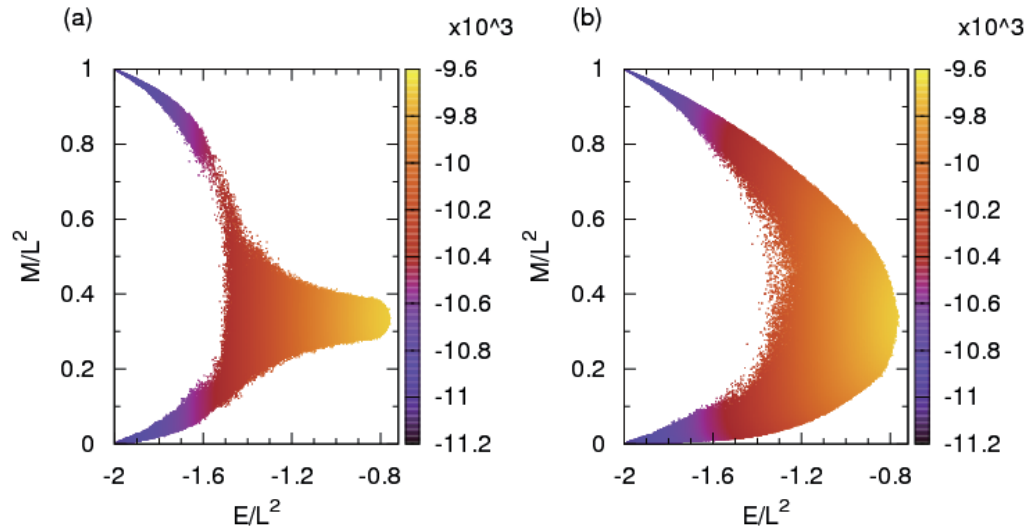


Figure 7. Calculated DOS obtained by WHAM with (a) ST and (b) STM data. The linear lattice size was $L = 80$.

only, and the white regions by neither of them. Thus, at first sight, it seems that there are some areas which are not particularly well sampled by the STM method and that ST may be somehow more powerful than STM.

Figure 9 zooms in on a region where blue is dominant (mainly sampled by ST). There are many pigments (in red and green) which both methods sampled and which even only STM sampled. This implies that because the ST method has more samples at a smaller number of parameter values, the part sampled is narrower but denser. However, the representative parts should be sampled properly by STM as well, although the sample density decreases.

To make sure that the STM method really samples the relevant areas sufficiently, we finally performed reweighting analyses along $h = 0$ with data obtained by ST and STM. Figures 10 and 11 show the specific heat C/L^2 and susceptibility χ/L^2 , respectively, as

Simulated tempering and magnetizing of a Potts model

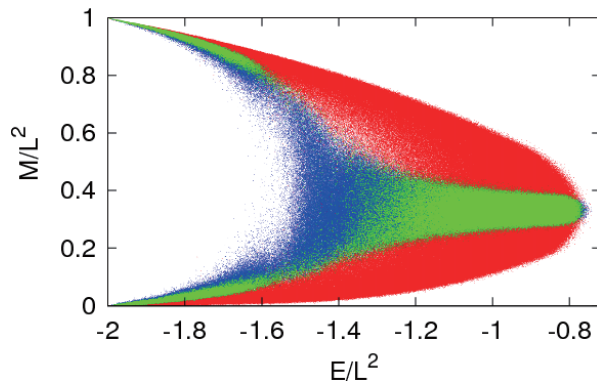


Figure 8. Difference in sampled points between ST and STM. The red, green, blue, and white regions correspond to the area sampled by only STM, by both of them, only by ST, and by neither of them, respectively ($L = 40$).

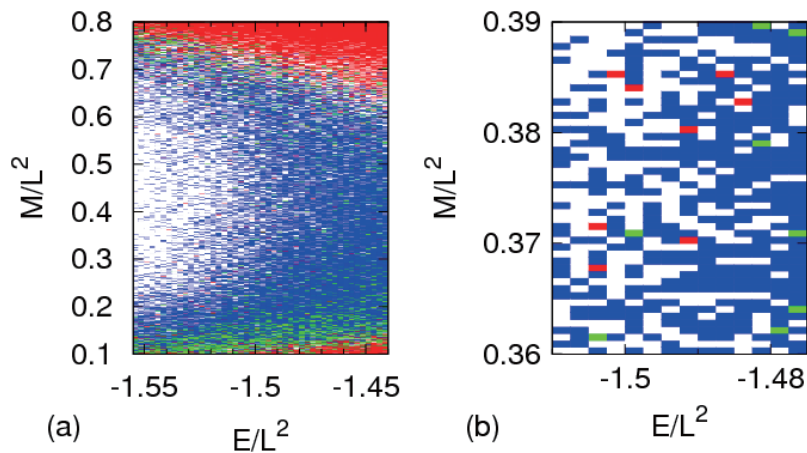


Figure 9. Zoom of the central (blue) region of figure 8 with increasingly higher resolution.

functions of T along the line $h = 0$. They are defined by

$$C \equiv \frac{\langle E^2 \rangle - \langle E \rangle^2}{T^2}, \quad (32)$$

$$\chi \equiv \frac{\langle M_{\max}^2 \rangle - \langle M_{\max} \rangle^2}{T}. \quad (33)$$

The red and green curves correspond to the data obtained by STM and by ST, respectively. The error bars were obtained by the jackknife method [38]–[41]. We do not observe pronounced differences between the two methods. Thus, we confirm that both methods let one sample the representative parts along $h = 0$ and that the STM method enables one to obtain the DOS in wider areas.

Because the STM method enables us to obtain the DOS in a wide range of sampling space, we can calculate the two-dimensional map of any thermodynamic quantity. Figure 12 shows the specific heat and susceptibility per spin as functions of T and h when

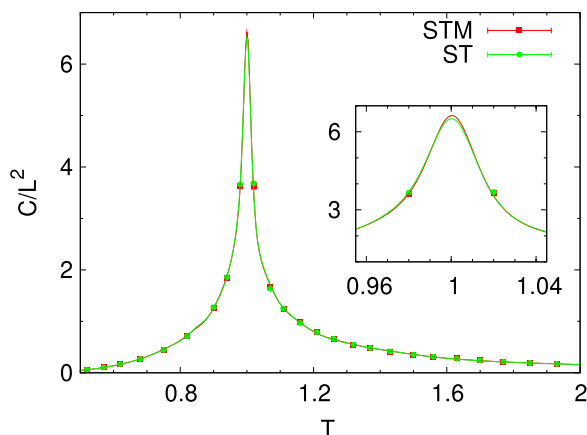


Figure 10. Specific heat C/L^2 as a function of T for $L = 40$. The inset shows the peak region with different abscissa and ordinate.

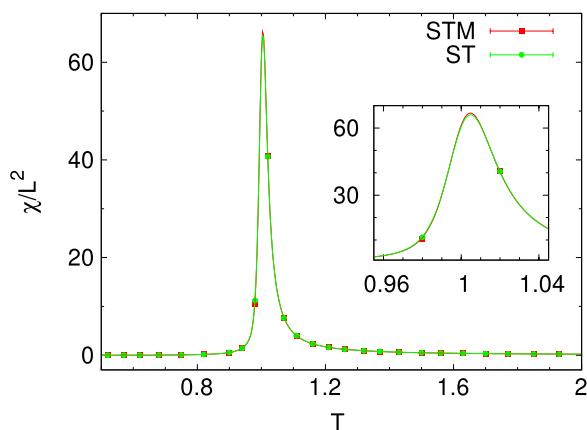


Figure 11. Susceptibility χ/L^2 as a function of T for $L = 40$. The inset shows the peak region with different abscissa and ordinate.

$L = 80$. This implies that the phase transition temperature converges to the Ising case value of 1.1346 as the external field becomes more and more negative. Related theoretical work can be found in, e.g., [42].

Figure 13 shows the specific heat as a function of temperature for some values of h and L . With positive external field, the phase transition disappears. However, because of finite-size effects, the abnormality, as measured by the diverging behavior, persists to some extent. With smaller external field, the diverging behavior remains for larger L . Vice versa, for larger L , the diverging behavior disappears more rapidly. This can be interpreted as a crossover between L and h .

Figure 14 shows the free energy per spin as a function of temperature and external field, which was obtained by applying MBAR to the results of the production runs. Note that the partial derivative of this free energy with respect to h gives $\langle M \rangle / TL^2$, where M is defined in (3). The shape at $h = 0$ suggests a jump of $\langle M \rangle$ below T_c , indicating the existence of first-order phase transitions.

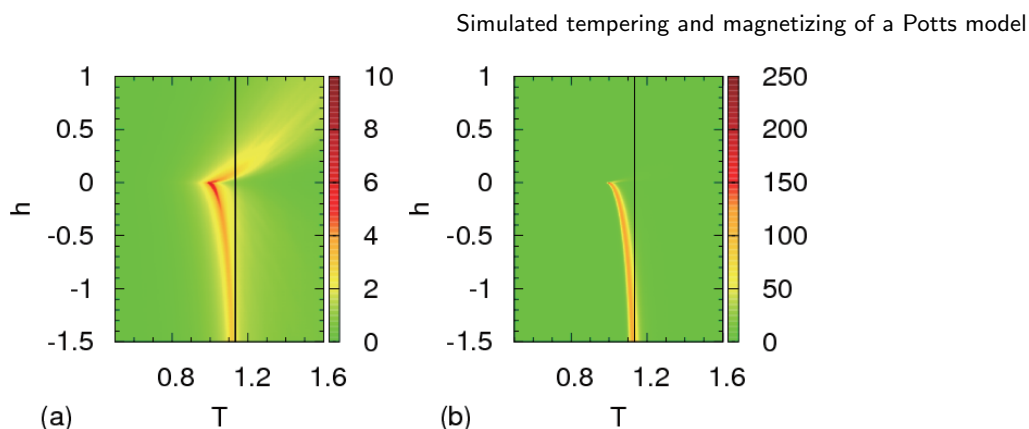


Figure 12. (a) C/L^2 and (b) χ/L^2 as functions of T and h for $L = 80$. The solid vertical line corresponds to $T = 1.1346$, which is the critical temperature of the Ising model (in the two-state Potts model normalization).

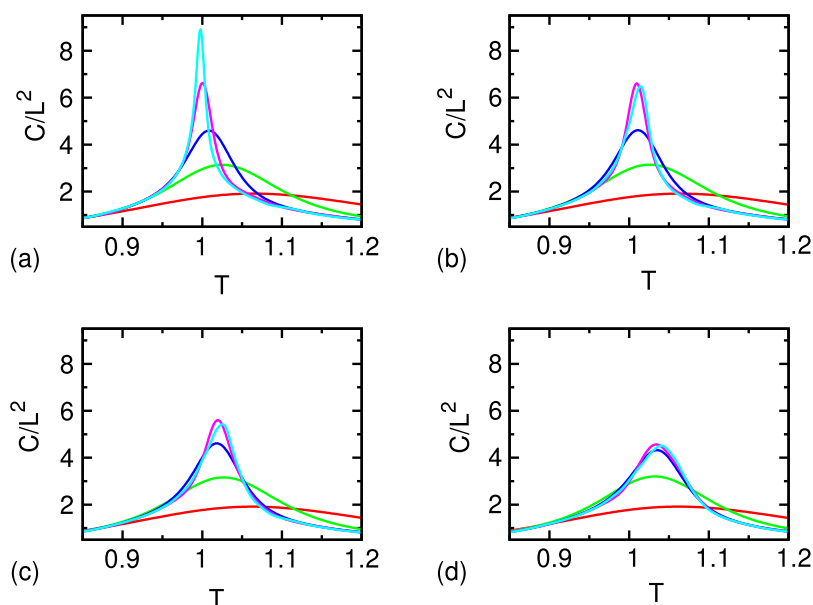


Figure 13. Specific heat C/L^2 as a function of T for $L = 5$ (red), 10 (green), 20 (blue), 40 (magenta), and 80 (cyan). (a) $h = 0.0$, (b) $h = 0.005$, (c) $h = 0.01$, (d) $h = 0.02$.

Finally to study the crossover behavior at the phase transitions, we calculated the magnetization by MBAR around the Potts critical point. The scaling form of the magnetization $m = M/L^2$ is given by [43]

$$mL^{\beta/\nu} = \Psi(tL^{y_t}, hL^{y_h}), \quad (34)$$

where $y_t = 1/\nu$ and $y_h = (\beta + \gamma)/\nu$. According to the crossover-scaling formalism [43], if $t^{-y_h/y_t} h$ (in the Potts model $t^{-14/9} h$) is small enough, then the magnetization obeys $m \sim t^\beta$ ($= t^{1/9}$), and if $h^{-y_t/y_h} t$ (in the Potts model $h^{-9/14} t$) is small enough (i.e., $t^{-14/9} h$ is large enough), then it obeys $m \sim h^{1/\delta}$ ($= h^{1/14}$), where $t = (T_c - T)/T_c$. For the Potts critical point, figure 15(a) shows that if the finite-size effects are negligible ($L^{6/5} t \gg 0.1$) and

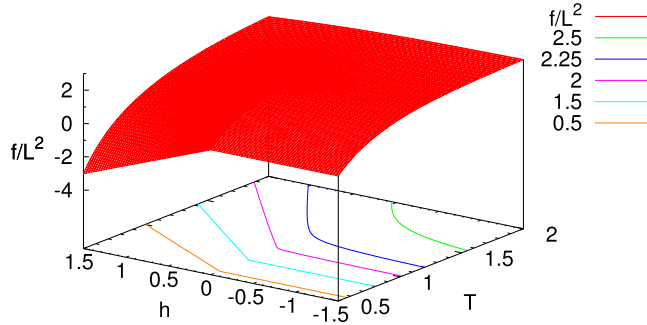


Figure 14. Free energy per spin f/L^2 and its contour curves as a function of T and h . The linear lattice size was $L = 80$.

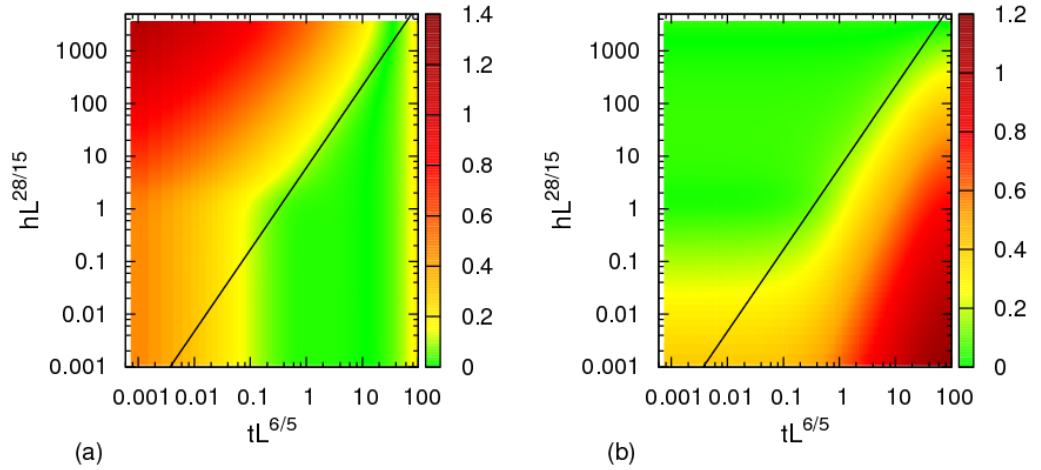


Figure 15. Difference between the magnetization and its expected scaling behaviors around the critical point for $L = 80$. Shown are (a) $|mL^{2/15} - 1.2(L^{6/5}t)^{1/9}|$ where the amplitude 1.2 was obtained by fitting the magnetization data to $t^{1/9}$ and (b) $|mL^{2/15} - (L^{28/15}h)^{1/14}|$. In both plots, the solid line corresponds to $h = 6t^{14/9}$.

$t \gg (h/6)^{9/14}$ (i.e., $t^{-14/9}h$ is small), then the critical behavior is $m \sim t^{1/9}$. Figure 15(b) shows that if finite-size effects are negligible ($L^{28/15}h \gg 0.1$) and $t \ll (h/6)^{9/14}$ (i.e., $t^{-14/9}h$ is large), then the critical behavior is $m \sim h^{1/14}$. Thus, figure 15 clearly shows that the line $h = 6t^{14/9}$ gives the boundary of the two scaling regimes.

Because the three-state Potts model in a negative external field is expected to behave like the Ising model, we also investigated the crossover behavior, between the two models. The scaling exponents of χ_{\max} for increasing L of the Potts model and the Ising model are given by $\gamma/\nu = 26/15$ and $7/4$, respectively. Figure 16 shows that the exponents are so similar that we cannot discern the difference, despite the accuracy of the measurements.

We hence also measured different quantities, which are the maximum values of $d \ln \langle m_{\max} \rangle / d\beta$, $d \ln \langle m_{\max}^2 \rangle / d\beta$, $d \ln \langle U_2 \rangle / d\beta$, $d \ln \langle U_4 \rangle / d\beta$, and $d \langle m_{\max} \rangle / d\beta$. Here, $U_2 = 1 - \langle m_{\max}^2 \rangle / 3 \langle m_{\max} \rangle^2$ and $U_4 = 1 - m_{\max}^4 / 3 \langle m_{\max}^2 \rangle^2$ are the Binder cumulants [44]. The derivatives were obtained by using [45]

$$\frac{d \ln \langle m_{\max} \rangle}{d\beta} = \langle E \rangle - \frac{\langle m_{\max} E \rangle}{\langle m_{\max} \rangle}, \quad (35)$$

Simulated tempering and magnetizing of a Potts model

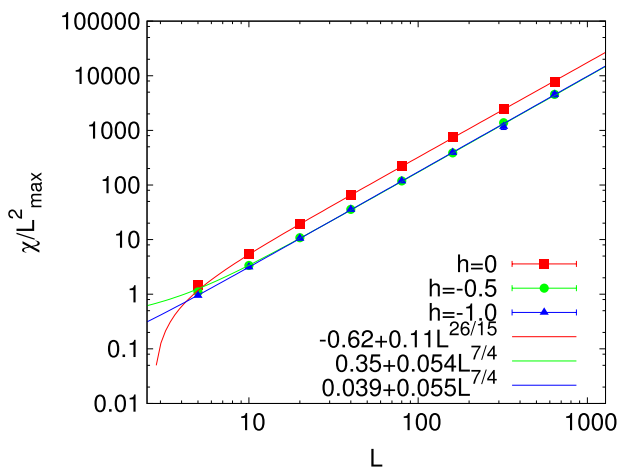


Figure 16. χ_{\max}/L^2 for three characteristic h values as functions of L .

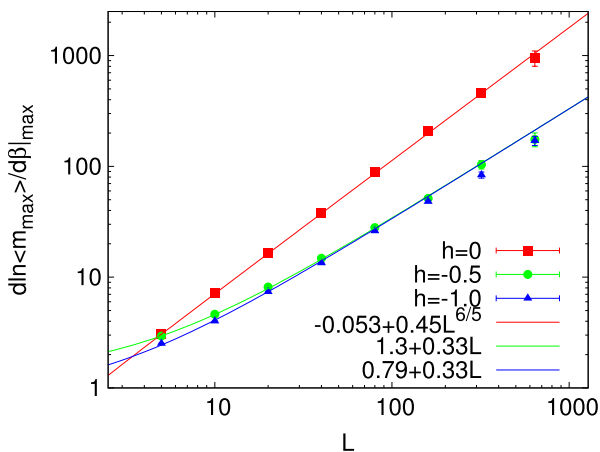


Figure 17. $d \ln \langle m_{\max} \rangle / d\beta|_{\max}$ for three characteristic h values as functions of L .

$$\frac{d \ln \langle m_{\max}^2 \rangle}{d\beta} = \langle E \rangle - \frac{\langle m_{\max}^2 E \rangle}{\langle m_{\max}^2 \rangle}, \quad (36)$$

$$\frac{d \ln \langle U_2 \rangle}{d\beta} = \frac{\langle m_{\max}^2 \rangle}{3 \langle m_{\max} \rangle^2} \left\{ \langle E \rangle - 2 \frac{\langle m_{\max} E \rangle}{\langle m_{\max} \rangle} + \frac{\langle m_{\max}^2 E \rangle}{\langle m_{\max}^2 \rangle} \right\}, \quad (37)$$

$$\frac{d \ln \langle U_4 \rangle}{d\beta} = \frac{\langle m_{\max}^4 \rangle}{3 \langle m_{\max}^2 \rangle^2} \left\{ \langle E \rangle - 2 \frac{\langle m_{\max}^2 E \rangle}{\langle m_{\max}^2 \rangle} + \frac{\langle m_{\max}^4 E \rangle}{\langle m_{\max}^4 \rangle} \right\}, \quad (38)$$

$$\frac{d \langle m_{\max} \rangle}{d\beta} = \langle m_{\max} \rangle \langle E \rangle - \langle m_{\max} E \rangle. \quad (39)$$

Figures 17–21 show our results. Note that $d \ln \langle m_{\max} \rangle / d\beta|_{\max}$, $d \ln \langle m_{\max}^2 \rangle / d\beta|_{\max}$, $d \ln \langle U_2 \rangle / d\beta|_{\max}$, $d \ln \langle U_4 \rangle / d\beta|_{\max}$, and $d \langle m_{\max} \rangle / d\beta|_{\max}$ are expected to behave asymptotically as $L^{1/\nu}$, $L^{1/\nu}$, $L^{1/\nu}$, $L^{1/\nu}$, and $L^{(1-\beta)/\nu}$, respectively, as the lattice size L increases [41]. These critical exponents are given for the Potts model by $\nu = \frac{5}{6}$ and $\beta = \frac{1}{9}$, so $(1 - \beta)/\nu = 16/15$, and for the Ising model by $\nu = 1$ and $\beta = \frac{1}{8}$, so $(1 - \beta)/\nu = 7/8$.

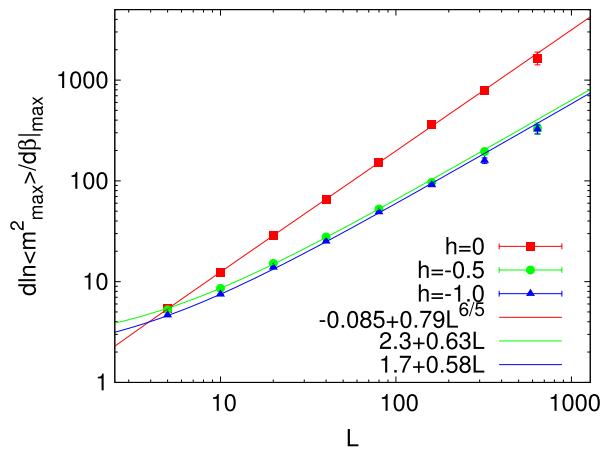


Figure 18. $d \ln \langle m_{\max}^2 \rangle / d\beta|_{\max}$ for three characteristic h values as functions of L .

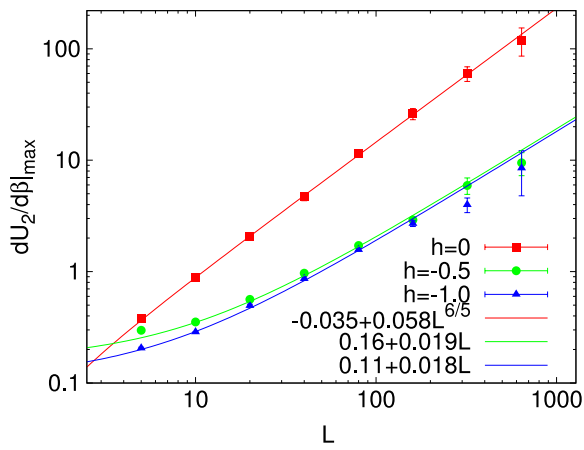


Figure 19. $d \ln \langle U_2 \rangle / d\beta|_{\max}$ for three characteristic h values as functions of L .

We observe that all quantities along $h = 0$ (the red curve with filled squares) follow the Potts case and that those for negative external field (green curve with filled circles and blue curve with filled triangles) follow the Ising case in the limit of large L . In fact, the two curves for $h = -0.5$ and -1.0 converge to almost the same line as L increases. On the other hand, the curve for $h = -0.5$ (green curve) shows more deviation from the scaling behavior for small L . This can also be understood as the crossover between L and h .

4. Conclusions

In this work, we applied the simulated tempering and magnetizing (STM) method [19, 20] to the two-dimensional three-state Potts model. During the simulations, two-dimensional random walks in temperature and external field were realized. The random walk covered a wide area of temperature and external field, so the STM simulations enabled us to study a wide area of the phase diagram from a single simulation run.

Because of the method's capability of dealing with a wider area of the sampling space (as is seen in the DOS), we can calculate thermodynamic quantities over an enlarged

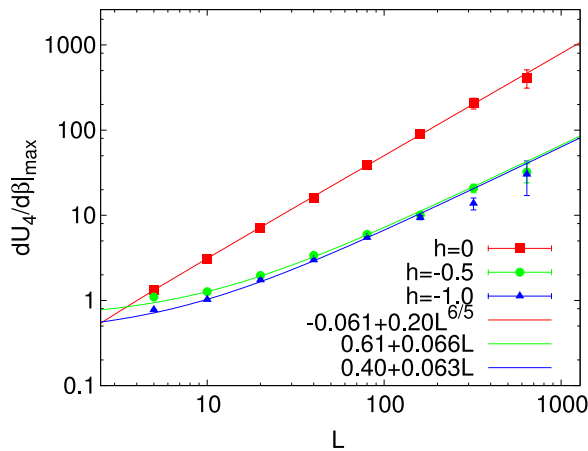


Figure 20. $d \ln \langle U_4 \rangle / d\beta|_{\max}$ for three characteristic h values as functions of L .

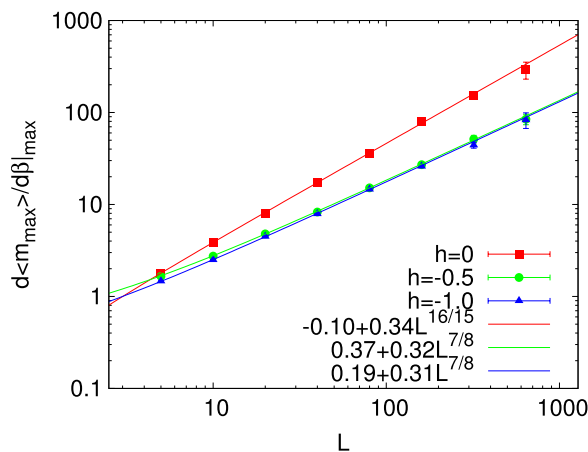


Figure 21. $d \langle m_{\max} \rangle / d\beta|_{\max}$ for three characteristic h values as functions of L .

range of the parameter space. We succeeded in reproducing many typical features of the system in the presence of an external field.

We calculated the magnetization and specific heat (and related quantities) as functions of temperature, external field, and lattice size around the critical point by reweighting techniques. The results allowed us to study the crossover behaviors of the phase transitions. From the magnetization, we observed a clear crossover between the scaling behaviors with respect to temperature and external field. From the specific heat and other quantities, the crossover in the scaling behavior with respect to external field and lattice size was also identified. The results all showed agreement with previous theoretical studies. Thus, this further supports the validity of STM.

With the data of the present work, we can calculate the two-dimensional density of states $n(E, M)$, so we can determine the weight factor for two-dimensional multicanonical simulations. By doing so, we can perform two-dimensional multicanonical simulations, which will be an interesting future task.

We finally remark that the present method is useful not only for spin systems but also for other complex systems with many degrees of freedom. Note also that because our

method does not require one to change the energy calculations, the method should be highly compatible with existing program packages.

Acknowledgments

Some of the computations were performed on the supercomputers at the Information Technology Center, Nagoya University, at the Research Center for Computational Science, Institute for Molecular Science, and at the Supercomputer Center, Institute for Solid State Physics, University of Tokyo. This work was supported, in part, by JSPS Institutional Program for Young Researcher Overseas Visits (to TN) and by Grants-in-Aid for Scientific Research on Innovative Areas ('Fluctuations and Biological Functions') and for the Computational Materials Science Initiative from the Ministry of Education, Culture, Sports, Science and Technology, Japan (MEXT). WJ gratefully acknowledges support by DFG Sonderforschungsbereich SFB/TRR 102 (Project B04) and the Deutsch-Französische Hochschule (DFH-UFA) under Grant No. CDFA-02-07. TN also thanks the Nagoya University Program for 'Leading Graduate Schools: Integrative Graduate Education and Research Program in Green Natural Sciences' for support of his extended stay in Leipzig.

References

- [1] Janke W, *Multicanonical Monte Carlo simulations*, 1998 *Physica A* **254** 164
- [2] Hansmann U H E and Okamoto Y, *The generalized-ensemble approach for protein folding simulations*, 1999 *Annual Reviews of Computational Physics VI* ed D Stauffer (Singapore: World Scientific) pp 129–57
- [3] Mitsutake A, Sugita Y and Okamoto Y, *Generalized-ensemble algorithms for molecular simulations of biopolymers*, 2001 *Biopolymers* **60** 96
- [4] Janke W (ed), 2008 *Rugged Free Energy Landscapes: Common Computational Approaches to Spin Glasses, Structural Glasses and Biological Macromolecules (Springer Lecture Notes in Physics)* vol 736 (Berlin: Springer)
- [5] Berg B A and Neuhaus T, *Multicanonical algorithms for first order phase transitions*, 1991 *Phys. Lett. B* **267** 249
- [6] Berg B A and Neuhaus T, *Multicanonical ensemble: a new approach to simulate first-order phase transitions*, 1992 *Phys. Rev. Lett.* **68** 9
- [7] Lyubartsev A P, Martsinovski A A, Shevkunov S V and Vorontsov-Velyaminov P N, *New approach to Monte Carlo calculation of the free energy: method of expanded ensembles*, 1992 *J. Chem. Phys.* **96** 1776
- [8] Marinari E and Parisi G, *Simulated tempering: a new Monte Carlo scheme*, 1992 *Europhys. Lett.* **19** 451
- [9] Hukushima K and Nemoto K, *Exchange Monte Carlo method and application to spin glass simulations*, 1996 *J. Phys. Soc. Japan* **65** 1604
- [10] Geyer C J, 1991 *Computing Science and Statistics, Proc. 23rd Symp. on the Interface* ed E M Keramidas (Fairfax, VA: Interface Foundation) pp 156–63
- [11] Wang F and Landau D P, *Efficient, multiple-range random walk algorithm to calculate the density of states*, 2001 *Phys. Rev. Lett.* **86** 2050
- [12] Wang F and Landau D P, *Determining the density of states for classical statistical models: a random walk algorithm to produce a flat histogram*, 2001 *Phys. Rev. E* **64** 056101
- [13] Laio A and Parrinello M, *Escaping free-energy minima*, 2002 *Proc. Nat. Acad. Sci. USA* **99** 12562
- [14] Swendsen R H and Wang J-S, *Replica Monte Carlo simulation of spin-glasses*, 1986 *Phys. Rev. Lett.* **57** 2607
- [15] Wang J-S and Swendsen R H, *Replica Monte Carlo simulation (revisited)*, 2005 *Prog. Theor. Phys. Suppl.* **157** 317
- [16] Mitsutake A and Okamoto Y, *From multidimensional replica-exchange method to multidimensional multicanonical algorithm and simulated tempering*, 2009 *Phys. Rev. E* **79** 047701
- [17] Mitsutake A and Okamoto Y, *Multidimensional generalized-ensemble algorithms for complex systems*, 2009 *J. Chem. Phys.* **130** 214105

- [18] Mitsutake A, *Simulated-tempering replica-exchange method for the multidimensional version*, 2009 *J. Chem. Phys.* **131** 094105
- [19] Nagai T and Okamoto Y, *Simulated tempering and magnetizing simulations of the Ising model*, 2012 *Phys. Proc.* **34** 100
- [20] Nagai T and Okamoto Y, *Simulated tempering and magnetizing: an application of two-dimensional simulated tempering to two-dimensional Ising model and its crossover*, 2012 *Phys. Rev. E* **86** 056705
- [21] Potts R B, *Some generalized order-disorder transformations*, 1952 *Math. Proc. Camb. Phil. Soc.* **48** 106
- [22] Wu F Y, *The Potts model*, 1982 *Rev. Mod. Phys.* **54** 235
- [23] Philipsen O, *The QCD phase diagram at zero and small baryon density*, 2006 29th Johns Hopkins Workshop on Current Problems in Particle Theory: Strong Matter in the Heavens PoS(JHW2005)012
- [24] Kim S, De Forcrand P, Kratochvila S and Takaishi T, *The 3-state Potts model as a heavy quark finite density laboratory*, 2005 arXiv:[hep-lat/0510069](https://arxiv.org/abs/hep-lat/0510069)
- [25] Karsch F and Stickan S, *The three-dimensional, three-state Potts model in an external field*, 2000 *Phys. Lett. B* **488** 319
- [26] Mercado Y D, Evertz H G and Gatteringer C, *Worm algorithms for the 3-state Potts model with magnetic field and chemical potential*, 2012 *Comput. Phys. Commun.* **183** 1920
- [27] Chodera J D and Shirts M R, *Replica exchange and expanded ensemble simulations as Gibbs sampling: simple improvements for enhanced mixing*, 2011 *J. Chem. Phys.* **135** 194110
- [28] Zhang C and Ma J, *Enhanced sampling and applications in protein folding in explicit solvent*, 2010 *J. Chem. Phys.* **132** 244101
- [29] Sindhikara D J, Meng Y and Roitberg A E, *Exchange frequency in replica exchange molecular dynamics*, 2008 *J. Chem. Phys.* **128** 024103
- [30] Sindhikara D J, Emerson D J and Roitberg A E, *Exchange often and properly in replica exchange molecular dynamics*, 2010 *J. Chem. Theory Comput.* **6** 2804
- [31] Matsumoto M and Nishimura T, *Mersenne twister: a 623-dimensionally equidistributed uniform pseudo-random number generator*, 1998 *ACM Trans. Model. Comput. Simul. (TOMACS)* **8** 3
- [32] Mitsutake A and Okamoto Y, *Replica-exchange simulated tempering method for simulations of frustrated systems*, 2000 *Chem. Phys. Lett.* **332** 131
- [33] Ferrenberg A and Swendsen R, *Optimized Monte Carlo data analysis*, 1989 *Phys. Rev. Lett.* **63** 1195
- [34] Kumar S, Bouzida D, Swendsen R H, Kollman P A and Rosenberg J M, *The weighted histogram analysis method for free-energy calculations on biomolecules. I. The method*, 1992 *J. Comput. Chem.* **13** 1011
- [35] Kumar S, Rosenberg J M, Bouzida D, Swendsen R H and Kollman P A, *Multidimensional free-energy calculations using the weighted histogram analysis method*, 1995 *J. Comput. Chem.* **16** 1339
- [36] Shirts M R and Chodera J D, *Statistically optimal analysis of samples from multiple equilibrium states*, 2008 *J. Chem. Phys.* **129** 124105
- [37] Mitsutake A, Sugita Y and Okamoto Y, *Replica-exchange multicanonical and multicanonical replica-exchange Monte Carlo simulations of peptides. I. Formulation and benchmark test*, 2003 *J. Chem. Phys.* **118** 6664
- [38] Miller R G, *The Jackknife—A Review*, 1974 *Biometrika* **61** 1
- [39] Efron B, 1982 *The Jackknife, the Bootstrap, and Other Resampling Plans* (Philadelphia, PA: SIAM)
- [40] Berg B A, 2004 *Markov Chain Monte Carlo Simulations and Their Statistical Analysis* (Singapore: World Scientific)
- [41] Janke W, *Monte Carlo methods in classical statistical physics*, 2008 *Lect. Notes Phys.* **739** 79
- [42] Sun G, *Interfacial tension of the three-state Potts model on a square lattice at a negative fields*, 1991 *Z. Phys. B* **82** 431
- [43] Fisher M E, *The renormalization group in the theory of critical behavior*, 1974 *Rev. Mod. Phys.* **46** 597
- [44] Binder K, *Finite size scaling analysis of Ising model block distribution functions*, 1981 *Z. Phys. B* **43** 119
- [45] Janke W, *Monte Carlo simulations in statistical physics—from basic principles to advanced applications*, 2012 *Order, Disorder and Criticality: Advanced Problems of Phase Transition Theory* vol 3, ed Y Holovatch (Singapore: World Scientific) pp 99–166